Hindawi
Advances in Polymer Technology
Volume 2019, Article ID 1098027, 10 pages
https://doi.org/10.1155/2019/1098027

Research Article

Fly Ash Particle Size Effect on Pore Structure and Strength of Fly Ash Foamed Geopolymer

Luchang Xiong,[1,2] Zhijun Wan ,[1,2] Yuan Zhang ,[1,2] Fangtian Wang,[1,2] Junhui Wang,[1,2] and Yanlei Kang[3]

[1]*Key Laboratory of Deep Coal Resource Mining (CUMT), Ministry of Education of China, Xuzhou 221116, China*
[2]*School of Mines, China University of Mining & Technology, Xuzhou 221116, China*
[3]*CHN ENERGY Investment Group Co., Ltd, Dananhu No. 1 Coal Mine, Hami 839000, China*

Correspondence should be addressed to Zhijun Wan; zhjwan@cumt.edu.cn

Received 20 August 2019; Accepted 16 September 2019; Published 29 December 2019

Guest Editor: Jianchao Cai

The aim of this paper is to study the particle size effect of fly ash (FLA) on pore structure and strength of Fly Ash Foamed Geopolymer (FAFG). Information on the macro-pores such as macro-pore size and distribution of FAFG is captured through binarization processing. Porosity and compressive strength of FAFG are respectively tested by Archimedes density test method and uniaxial compressive strength test method. It can be concluded that the FLA particle size has an effect on the pore structure and strength of FAFG. More specifically, the effect of FLA particle size shows itself macroscopically on the quantity of middle and large macro-pores and the uniformity of macro-pores distribution, and microscopically on the quantity of micro-holes and cracks and calcium silicate (C-S-H) quantity at the early stage of FAFG mixture. All of the properties of FAFG follow some kind of changing rule except at the turning point when FLA particle is of 0.125~0.25 mm in size. To explain clearly the root cause of FLA particle size effect on FAFG, SEM, and XRD are employed to explore the microstructure of FAFG and the component of FLA. It turns out to be the amorphous phase SiO_2 content in FLA of different particle sizes which could determine the reaction extent of FAFG mixture.

1. Introduction

Coal combustion or the co-firing of biomass and coal has encountered certain operational problems, such as ash deposits, slagging, fouling and corrosion, reducing the thermal efficiency of boilers [1, 2], and resulted in problems in solid waste disposal, which is a long-stand research hotspot. As the largest amount of solid waste produced by rapid oxidation of coal powder during thermal power generation [3], Fly ash (FLA) pollutes the local environment and increases the cost of the treatment for coal mine. On the other hand, because of its advantages like good thermal insulation, light weight, and low cost [4, 5], FLA has been widely used in some architectural fields like nonbearing wall construction, bathroom backfilling and as functional materials such as thermal insulation material, sound-insulation material, and so on [6, 7]. Apart from being used in the traditional building fields, FLA has been applied in different areas as a good raw material for the preparation of geopolymer [8–12]. For example, to prove the possibility of in-situ resource utilization of FLA, there are a good many scholars having done plenty of basic studies on this aspect [13–15], among which there is one proposing that fly ash foamed geopolymer (FAFG) as backfilling material can be an excellent combination of fly ash consumption and coal mine fire prevention [16, 17]. The complex underground environment demands highly for some specific properties of FAFG, mainly focusing on its pore structure and strength.

As for the preparation of FAFG, the most significant point is to stabilize the suitable pore structure and generate appropriate strength, which are affected by different factors such as temperature, components, active materials, and so on [18–21]. However, there are few studies on FLA particle size effect on the properties of FAFG and the root cause for the effect has not been made clear yet. But plenty of FAFG preparation experiments have made it evident that the different FLA particle sizes do have some influence on the property of FAFG. The main objectives of this research are to observe the FLA particle size effect on the properties of FAFG and to investigate the root cause for the effect.

In terms of the way of foam generation, FAFG can be divided into two categories: mechanical foamed-FAFG [22,

Figure 1: Pictures of fly ash through particle size classification from Dananhu coal mine no. 1.

23] and chemical foamed-FAFG [24, 25], which are respectively produced by special foaming machine with some kind of foaming agent and by finely divided aluminum or hydrogen peroxide [26, 27]. In this research, FAFG was made of FLA of different particle sizes and other raw materials in the form of chemical foaming with hydrogen peroxide. With the high-quality pictures taken by SLR camera, macro-pore structure characteristics were measured through binarization processing analysis. XRD and SEM were employed to determine the components of FLA and to observe the micro-pore structure of FAFG respectively. The uniaxial compressive strength was tested by the universal testing machine. The novelty of my research lies firstly in the investigation of the FLA particle size effect on the properties of FAFG, and secondly in the finding of the root case for this effect. The components of FLA changed with the particle size, which resulted in different performances and different degrees of strength of macro- and micro- scale pore structure accordingly. It turns out that the crystal/amorphous ratio might be the root cause for the effect.

2. Materials and Methods

2.1. Materials. As is shown in Table 1, fly ash of six size ranges were obtained through using vibrating screen, and they are respectively −0.045 mm, 0.045~0.075 mm, 0.075~0.125 mm, 0.125~0.25 mm, 0.25~0.5 mm, and +0.5 mm. Pictures of fly ash through particle size classification from Dananhu coal mine no.1 are shown in Figure 1. Except for the max size (+0.5 mm) and the min size (−0.045 mm), the fly ash graded by size was used as the raw material for FAFG. Detailed information on other raw materials and additives are listed in Table 2.

Table 1: Particle size classification of fly ash from Dananhu no.1 coal mine.

Size/(mm)	Mass fraction/(%)	Add up/(%)
−0.045	47.03	47.03
0.045–0.075	10.60	57.63
0.075–0.125	20.02	77.65
0.125–0.25	15.00	92.65
0.25–0.5	6.60	99.25
+0.5	0.75	100

2.2. Experimental Procedure. Based on the experience from a trial and error approach in the early stage, the mixed proportion of FAFG was obtained, which is shown in Table 3. All of the FAFG mixtures were prepared according to the uniform ratio, of which the only difference was the grading size of the fly ash. To obtain the initial samples, the mixtures were cast in steel cubic molds (100 mm), foaming naturally because of the inside reaction of hydrogen peroxide. The foaming period lasted about a quarter of an hour, and then the samples were left at 100°C in a thermostatic heater for 2 hours; the consolidation was completed in a room with temperature of 22–24°C till the day for testing. The central cubes (70.7 mm) incised from the untreated samples (100 mm) were prepared for the microstructure observation, porosity measurement

Table 2: Raw materials for FAFG.

Material	Chemical formula	Function	Purity	Origin
FLA	—	Cementitious materials	—	Dananhu no.1 Coal Mine, Hami, Xinjiang, China
CC	—	Cementitious materials	—	Yanhang Mineral Products Trading Co., Ltd., Shijiazhuang, Hebei, China
SH	NaOH	Alkali activator	>96%	Bohe Fine Chemicals Co., Ltd., Shanghai, China
SS	Na_2SO_4	Sulfate activator	>96%	Sinopharm Chemical Reagent Co. Ltd., Shanghai, China
CO	CaO	Reinforcing agent	>98%	Sinopharm Chemical Reagent Co., Ltd., Shanghai, China
CS	$C_{36}H_{70}CaO_4$	Foam stabilizer	98%	Chemical Technology Co., Ltd., Shanghai, China
HP	H_2O_2	Foaming agent	Mass fraction = 30%	Zhenqi Fine Chemicals Co., Ltd., Shanghai, China

FLA – Fly ash; CC – Cement clinker; SH – Sodium hydroxide; CO – Calcium oxide; SS – Sodium sulfate; CS – Calcium stearate; HP – Hydrogen peroxide; W – Water.

Table 3: Mix proportion of raw material for FAFG (kg/batch).

Samples	FLA	CC	SH	CO	SS	CS	FA	W	Particle size of FLA (mm)
FAFGs1	1	1	0.04	0.04	0.02	0.02	0.14	0.72	0.045~0.075
FAFGs2	1	1	0.04	0.04	0.02	0.02	0.14	0.72	0.075~0.125
FAFGs3	1	1	0.04	0.04	0.02	0.02	0.14	0.72	0.125~0.25
FAFGs4	1	1	0.04	0.04	0.02	0.02	0.14	0.72	0.25~0.5

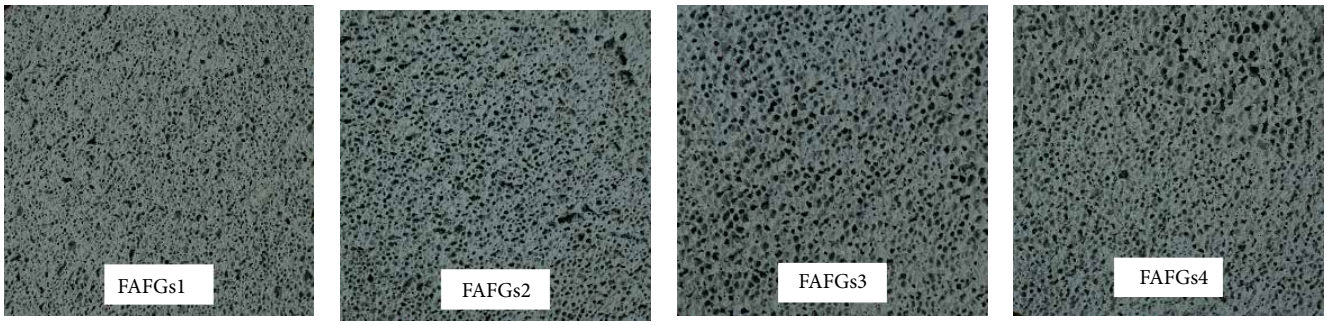

(a) (b) (c) (d)

Figure 2: Incised central cubes of FAFG.

and strength testing. The central cubes incised are shown in Figure 2.

2.3. Test Method. The X-ray diffraction diffractometer (XRD Bruker D8 Advance) was employed to determine the crystalline phase of FLA. The pore morphology pictures of FAFG samples were obtained through the digital single lens reflex (Nikon D5500). With the help of open source software (Image-Pro Plus), the pore size distribution of FAFG samples was analyzed through employing image binarization processing for the pore morphology pictures. The strength testing of FAFG samples was carried out using the universal testing machine (WDW-300). The microstructure of FAFG samples was observed through scanning electron microscope (SEM, ZEISS SIGMA-300). The bulk density of FAFG samples was measured using the standard Archimedes method with distillated water. The total porosity was calculated according to the following Equation (1):

$$P = \left(\frac{\rho_0 - \rho}{\rho_0}\right) * 100\%, \quad (1)$$

where ρ and ρ_0 represents the bulk density and powder density, respectively.

3. Result and Discussion

3.1. Pore Structure Analysis. To some extent, the cross section of the incised central cubes could reflect the real inner pore structure of FAFG, and therefore, the Nikon D5500 was used to obtain a high resolution image of the cube side. Pore structure data was analyzed after binarization processing [28] using the open source software "Image Pro Plus". Raw picture and picture after binarization processing are respectively shown in Figure 3 where pore structure and its distribution can be clearly seen.

Diameter is one of the main characteristic parameters of pore structure, but there are few completely suitable classification standards for such porous materials as aerated or foamed geopolymer (concrete) of largescale (μm~mm). Most of classification standards or methods existing [29] are based on the standard of IUPAC in which there is only

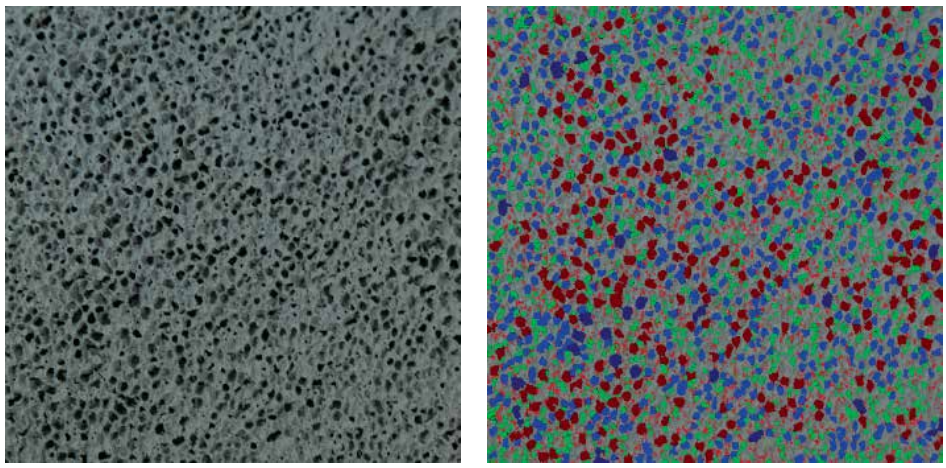

(a) (b)

Figure 3: Cross section picture before (a) and after (b) binarization processing.

Table 4: Summary of the most frequently used pore size classifications [30].

Classification	Specified types of pores, d [nm]					
	Macro-	Meso-	Micro-	Supermicro-	Ultramicro-	Submicro-
IUPAC	>50	2 ÷ 50	<2	0.7 ÷ 2	<0.7	<0.4
Dubinin	>200 ÷ 400	200 ÷ 400 > d > 3 ÷ 3.2	<1.2 ÷ 1.4	3 ÷ 3.2 > d > 1.2 ÷ 1.4	—	—
Cheremskoj	>2000	—	2000 > d > 200	—	<2 ÷ 4	<200
Kodikara	$10^4 \div 10^6$	—	$10^3 \div 3 \times 10^4$	$25 \div 10^3$	<3 ÷ 4	—

classification of the nanoscale pores but no more classification of largescale ones (>50 nm). Zdravkov et al [30] generalized the most frequently used pore size classifications shown in Table 4 in which the classification of Kodikara et al. [31] is more suitable for classifying largescale pores. According to Kodikara's classifying standard, all the pores observed in FAFG in this study should be categorized as macro-pores, with pores ($d > 10^6$ nm) being excluded. In this study, macro-pore diameter was divided into 5 grades at four intervals and each interval was 0.5 mm in length; however, it could not reflect the difference in pore size visually. Therefore, macro-pores of grade I and II could be defined as small ones (0 mm $\leq d <$ 1mm), macro-pores of grade III and IV as middle ones (1 mm $\leq d <$ 2mm), and macro-pores of grade V as large ones ($d \geq$ 2mm). Figure 4 shows the pore size distribution of FAFG. It is evident from Figure 4 that almost all of the pore size distribution concentrated in small pore, but there is still sporadic pore size in middle and large pore. With the enlargement of FLA particle size, the middle and large pore quantity of FAFGs1, FAFGs2, and FAFGs3 increase, yet there is no more growth but decrease when it comes to FAFGs4. At the same time, trace of large pore which can hardly be found in the first three kinds of FAFG appears quite distinct in FAFGs4.

3.2. Strength Development. Figure 5 shows the result of compressive strength test and porosity determination for FAFG. The early age strength ranges from 0.097 MPa to 0.3241 MPa (percentage difference: 70%), which means the strength difference of FAFG of different FLA particle sizes is large. The porosity ranges from 66.37% to 73.15%, leading to FAFG density range from 300 to 500 kg/m^3. As can be seen in Figure 5, with the enlargement of FLA particle size, the compressive strength (7d) decreases and the porosity increases. FAFGs3 is still a turning point where the compressive strength arrives at the bottom and the porosity reaches the peak, and the porosity stops to rise and begins to decrease while the compressive strength shows the converse change. There are many studies on the relationship between porosity and strength, and almost all of their conclusions point out that large porosity means bad strength performance [21, 32]. Two main factors could be used to explain the connection between strength and pore structure; one is the free volume of pores (porosity) and the other is the single pore size (heterogeneously distributed large pores). Both of them are related to FLA particle size. With the enlargement of FLA particle size, the quantity of heterogeneously distributed large macro-pores and the porosity of FAFG increases first and then decreases, as can be respectively seen in Figures 2 and 5. Because of the negative impact of these two factors on strength of FAFG, the compressive strength of FAFG shows a variation trend opposite to that of the two factors.

3.3. XRD Analysis. "Fly ash effect" refers to a series of effects including morphological effect, micro-aggregate effect and active effect. With the enlargement of FLA particle size, the morphological effect and micro-aggregate effect weaken obviously, which might result in some bad impact on FAFG such as more heterogeneous pore distribution, larger porosity and worse strength performance. FAFGs1, FAFGs2, and

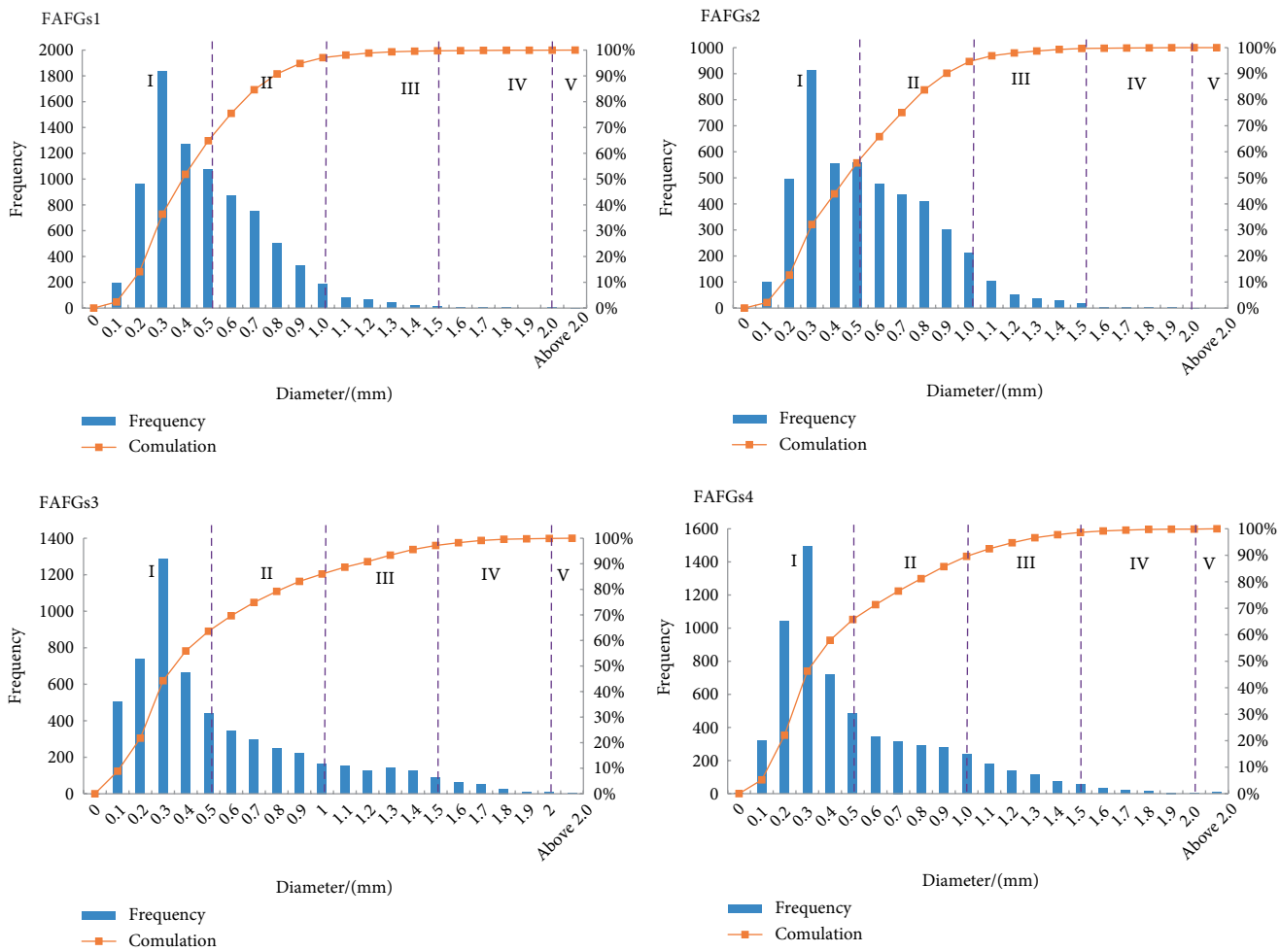

Figure 4: Pore size distribution of FAFG.

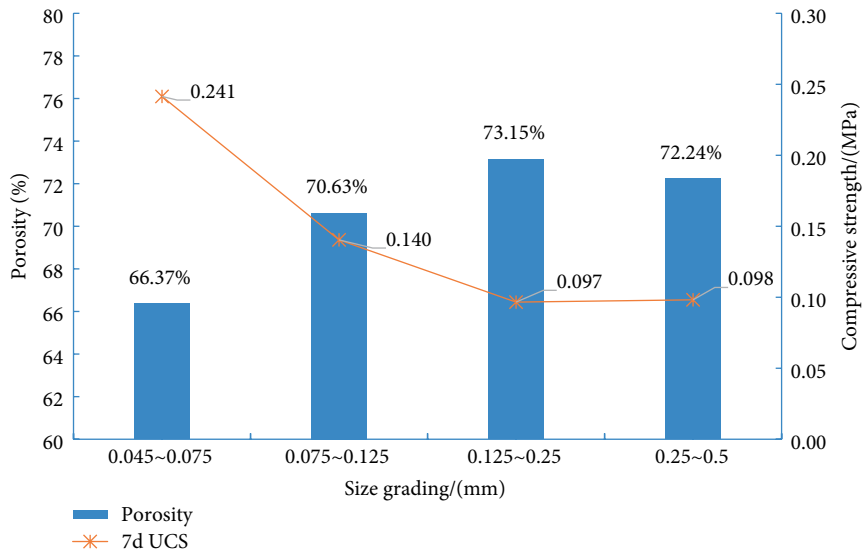

Figure 5: Curve of porosity and compressive strength to size grading.

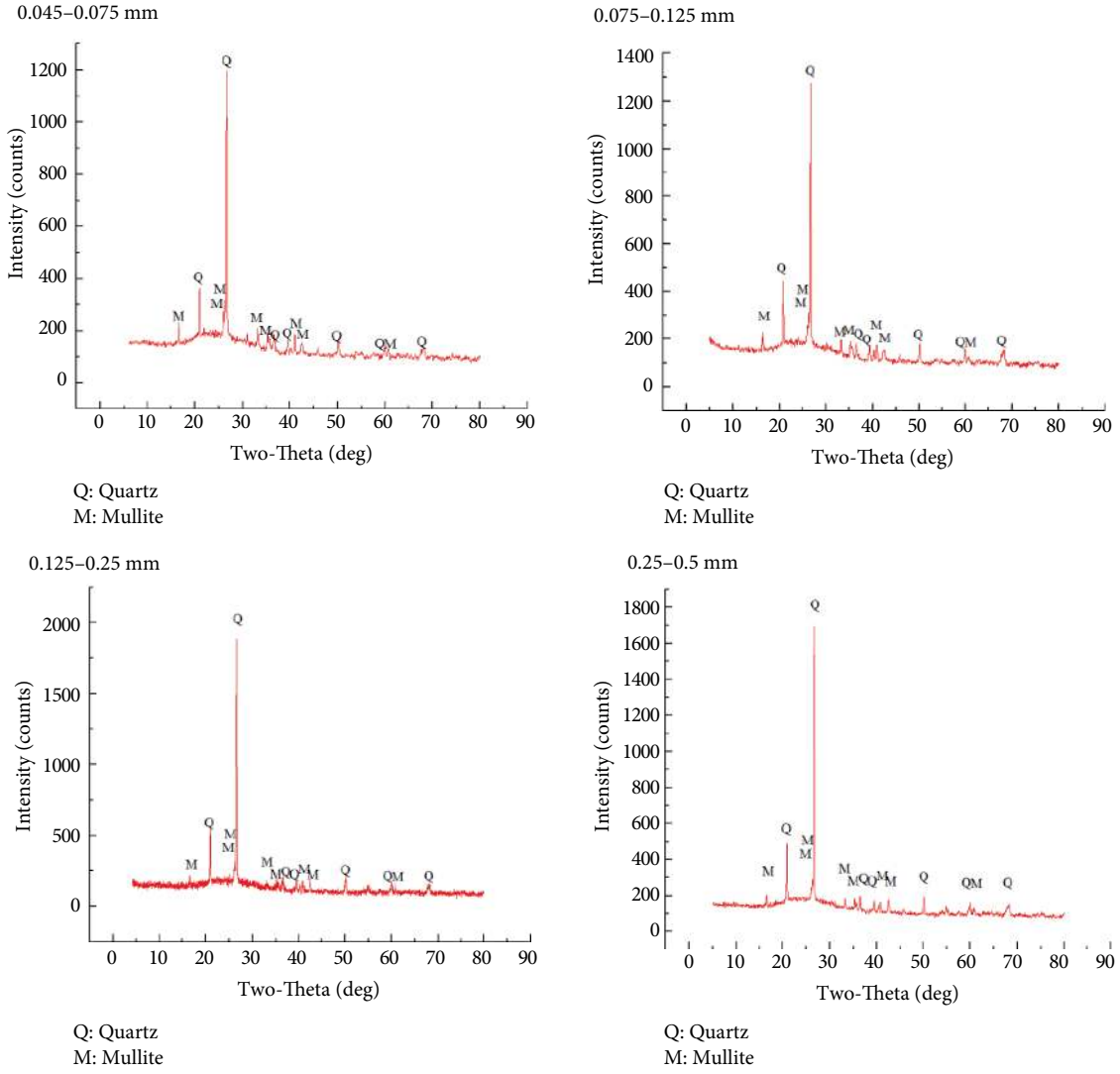

Figure 6: XRD pattern of fly ash with different particle sizes.

FAFGs3 accord well with this changing rule as expected, yet FAFGs4 does not follow this changing rule.

To figure out why there is at FAFGs3 always a turning point which leads to the appearance of all these strange phenomena. XRD analysis was conducted on fly ash of different particle sizes. Figure 6 shows the XRD analysis result. As can be seen in the Figure 6, Quartz and Mullite are the main components of FLA. A big "steamed bread peak" appears at the degree of 20~30°; meanwhile, as FLA particle size enlarges, the "teamed bread peak" becomes bigger firstly and smaller then. Size of the "steamed bread peak" reflects the amorphous phase mineral content. The bigger the size of "steamed bread peak" is, the more amorphous phase SiO_2 there is; Taylor and Matulis pointed out that peak heights can proportionally characterize the peak areas when it comes to well-defined peaks without significant peak width [33]. Liu compared the silica content of aluminosilicate with different sources by comparing their peak intensity [34]. Diffraction intensity can reflect the crystal phase mineral content, and therefore, peak diffraction intensity of SiO_2 is conducive to acquisition of crystal phase

Table 5: SiO_2 peak intensity of fly ash with different particle sizes.

Particle size/(mm)	0.045~0.075	0.075~0.125	0.125~0.25	0.25~0.5
Peak intensity	1269	1373	1887	1758

SiO_2 content. As can be seen in Table 5, the peak diffraction intensity of SiO_2 first increases and then decreases with the enlargement of FLA particle size.

Figure 7 represents the planar model of molecular structure of crystal phase SiO_2 and amorphous phase SiO_2. As can be seen in the figure, the molecular structure of crystal phase SiO_2 was much more compact and orderly than that of amorphous phase SiO_2, which means Si-O bonds of the former were more firmly structured than those of the latter, and that the latter was easier to break by alkaline activator in FAFG mixture. Tennakoon reasoned that amorphous phase SiO_2 was the key to produce reactive SiO_2 in geopolymer formation [35]. Because the crystal phase SiO_2 was inert constituent of the

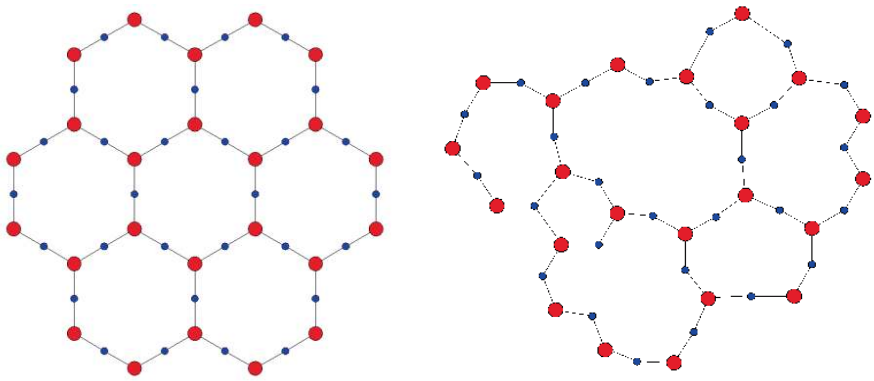

Crystal phase SiO_2 Amorphous phase SiO_2

FIGURE 7: Planar model of molecular structure of SiO_2.

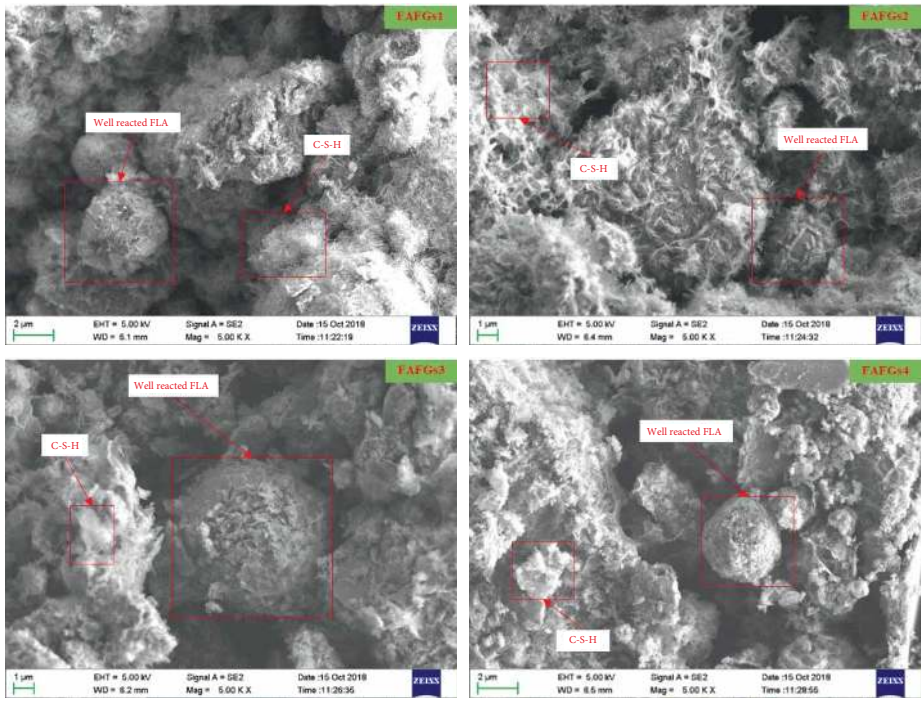

FIGURE 8: SEM result for reaction extent of FAFG.

hydration reaction of FAFG, there is a negative impact on the pore formation and distribution. Molecular structure of amorphous phase SiO_2 can be easily broken in the alkaline environment, so that the activated SiO_2 could restructured with some other materials in the FAFG mixture; for example, it can react with calcium hydroxide produced by hydration reaction of calcium oxide. This contributes to the uniform spatial and size distribution of pores.

3.4. SEM Analysis. Figure 8 shows the SEM (test condition: ETH = 5 kV, Signal A = SE2, Mag = 5.00 KX) figure of FAFG. The original appearance of raw fly ash is a smooth sphere, but many flocs appear on its surface after raw fly ash reacts in the FAFG mixture. After being activated by the alkaline activator, amorphous phase SiO_2 reacts with the Ca^{2+} provided by CC and CO, leading to the forming of a large amount of C-S-H (Calcium silicate hydrate) on the surface of FLA particle. There is often a considerable quantity of Cubilose-shaped or vermicular-shaped C-S-H existing in the fly ash-lime-water hardenite. From Figure 8, it can be clearly seen that the quantity of flocs first decreases and then increases with the enlargement of FLA particle size, whose turning point is still FAFGs3. C-S-H is the main product of FAFG, and the quantity of C-S-H could represents the extent of reaction. Therefore, the reaction extent of FAFG mixture changes with the enlargement of FLA particle size. The change of amorphous phase SiO_2 with the FLA particle size is the root cause of the change of reaction extent, and strength of FAFG becomes stronger due to the formation of C-S-H in the early stage.

Microscale cracks and holes can be observed with the help of SEM. Figure 9 shows SEM (test condition: ETH = 5 kV, Signal A = InLens, Mag = 5.00 KX) figure of FAFG. As can be seen in

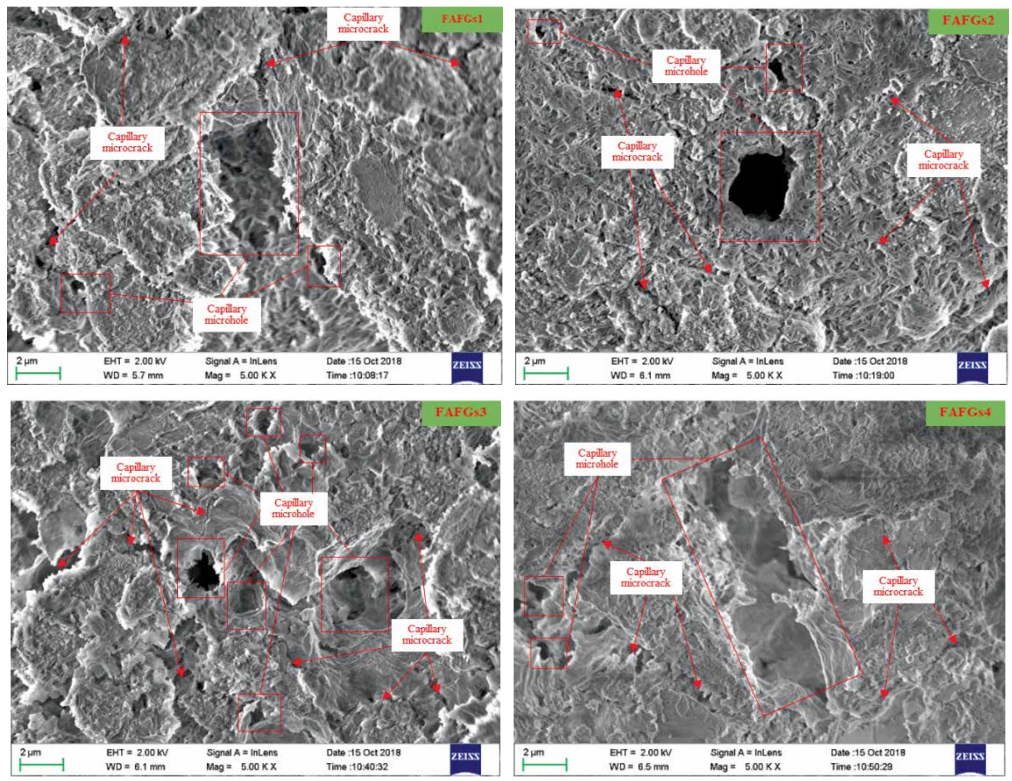

Figure 9: SEM result for micro-cracks & micro-holes of FAFG.

the figure, there are plenty of micro-cracks and micro-holes in FAFG. It is obvious that the quantity of the crack and hole first increases and then decreases as the FLA particle size enlarges. During the reaction process, actived SiO_2 could easily react with Ca^{2+} and form hardenite early with which the tiny foam cannot merge into big ones. Meanwhile merging of tiny foams can increase the inner air preasure of foam, leading to the appearance of micro-cracks. It can be concluded that the FLA particle size has an indirect impact on micro-crack and micro-hole formation of FAFG due to the content of amorphous phase SiO_2. Micro-cracks and micro-holes existing in FAFG might have a negative effect on the strength of FAFG, because they could weaken the hardenite structure. FLA with more amorphous phase SiO_2 might contribute to the formation of more evenly distributed pore and better strength performance of FAFG.

4. Conclusions

Generally speaking, with the enlargement of FLA particle size, the UCS of FAFGs decreases first and then increases, and the porosity and the quantity of middle and large macro-pores increases first and then decreases. Besides, 0.125~0.25 mm is the turning point for both of them. Uniformity of pore distribution gets worse as the FLA particle size enlarges, but it turns better when it comes to 0.25~0.5 mm. According to the micro analysis, with the enlargement of FLA particle size, the content of C-S-H (reaction product of FAFG mixture) decreases first and then increases, and the quantity of micro-pores and cracks increases first and then decrease and their turning points are also 0.125~0.25 mm.

Results in this study show that the FLA particle size has an effect on the pore structure and strength of FAFG, and the root cause for the effect is the content difference of active substance (amorphous phase SiO_2), and the difference is triggered by changes in particle size after sieving. XRD results show that amorphous phase SiO_2 content of FLA decreases first and then increases with the enlargement of FLA particle size with a turning point as 0.125~0.25 mm, which means FLA of particle size of 0.125~0.25 mm has the least content of active substance. The content of active substance could determine the reaction extent of FAFG mixture. In short, a fuller reaction of the mixture will would produce more C-S-H and less micro-holes and cracks, bringing a better strength performance and more uniform pores of FAFG.

Data Availability

No data were used to support this study.

Conflicts of Interest

The authors declare that they have no conflicts of interest.

Acknowledgments

This work has been supported by the major projects of National Natural Science Foundation of China (51674242, 51974297).

Supplementary Materials

The graphical abstract introduces preparation process of (fly ahs foamed geopolymer) FAFG and some characteristcs testing for FAFG. The whole preparation process includes dry raw materials mixing, alkali-activator adding, foaming and curing. Then the FAFG samples will be incised into cubes (70.7 mm). Finally characteristics of FAFG will be tested with relevant instruments and methods. (*Supplementary Materials*)

References

[1] X. Yao, H. Zhou, K. Xu, Q. Xu, and L. Li, "Evaluation of the fusion and agglomeration properties of ashes from combustion of biomass, coal and their mixtures and the effects of K_2CO_3 additives," *Fuel*, vol. 255, p. 115829, 2019.

[2] X. Yao, H. Zhou, K. Xu, Q. Xu, and L. Li, "Investigation on the fusion characterization and melting kinetics of ashes from co-firing of anthracite and pine sawdust," *Renewable Energy*, vol. 145, pp. 835–846, 2020.

[3] S. Wang and G. Sun, "Analysis of the relationship among thermal power generation, coal-fired consumption and sulfur dioxide emission in China during 1991–2007," *Resources Science*, vol. 32, no. 7, pp. 1230–1235, 2010.

[4] M. Ahmaruzzaman, "A review on the utilization of fly ash," *Progress in Energy & Combustion Science*, vol. 36, no. 3, pp. 327–363, 2010.

[5] G. Ferraiolo, M. Zilli, and A. Converti, "Fly ash disposal and utilization," *Journal of Chemical Technology & Biotechnology Biotechnology*, vol. 47, no. 4, pp. 281–305, 2010.

[6] P. Padevět and O. Zobal, "Influence of humidity on the material properties of cement paste with fly ash in the mutual relation 50/50," *Applied Mechanics and Materials*, vol. 486, pp. 327–332, 2013.

[7] Z. Lei, S. Quan, and L. Ping, "Research on preparation of porous materials by fly ash and corn fiber," in *2011 International Symposium on Water Resource & Environmental Protection*, IEEEXi'an, China, 2011.

[8] Z. Zhang, Y. Zhu, H. Zhu, Y. Zhang, J. L. Provis, and H. Wang, "Effect of drying procedures on pore structure and phase evolution of alkali-activated cements," *Cement and Concrete Composites*, vol. 96, pp. 194–203, 2019.

[9] H. Alanazi, J. Hu, and Y.-R. Kim, "Effect of slag, silica fume, and metakaolin on properties and performance of alkali-activated fly ash cured at ambient temperature," *Construction and Building Materials*, vol. 197, pp. 747–756, 2019.

[10] M. Khedmati, H. Alanazi, Y.-R. Kim, G. Nsengiyumva, and S. Moussavi, "Effects of Na_2O/SiO_2 molar ratio on properties of aggregate-paste interphase in fly ash-based geopolymer mixtures through multiscale measurements," *Construction and Building Materials*, vol. 191, pp. 564–574, 2018.

[11] N. A. Farhan, M. N. Sheikh, and M. N. S. Hadi, "Investigation of engineering properties of normal and high strength fly ash based geopolymer and alkali-activated slag concrete compared to ordinary Portland cement concrete," *Construction and Building Materials*, vol. 196, pp. 26–42, 2019.

[12] M. N. S. Hadi, H. Zhang, and S. Parkinson, "Optimum mix design of geopolymer pastes and concretes cured in ambient condition based on compressive strength, setting time and workability," *Journal of Building Engineering*, vol. 23, pp. 301–313, 2019.

[13] L. Biondi, M. Perry, C. Vlachakis, Z. Wu, A. Hamilton, and J. McAlorum, "Ambient cured fly ash geopolymer coatings for concrete," *Materials*, vol. 12, no. 6, p. 923, 2019.

[14] S. Parvathy S, A. K. Sharma, and K. B. Anand, "Comparative study on synthesis and properties of geopolymer fine aggregate from fly ashes," *Construction and Building Materials*, vol. 198, pp. 359–367, 2019.

[15] A. B. Malkawi, H. Al-Mattarneh, B. E. Achara, B. S. Mohammed, and M. F. Nuruddin, "Dielectric properties for characterization of fly ash-based geopolymer binders," *Construction and Building Materials*, vol. 189, pp. 19–32, 2018.

[16] W. Di, B. Yang, and Y. Liu, "Transportability and pressure drop of fresh cemented coal gangue-fly ash backfill (CGFB) slurry in pipe loop," *Powder Technology*, vol. 284, pp. 218–224, 2015.

[17] H. Wen, D. Zhang, Z. Yu, X. Zheng, S. Fan, and B. Laiwang, "Experimental study and application of inorganic solidified foam filling material for coal mines," *Advances in Materials Science and Engineering*, vol. 2017, Article ID 3419801, 13 pages, 2017.

[18] M. Mahdavi, O. Yousefzade, and H. Garmabi, "A simple method for preparation of microcellular PLA/calcium carbonate nanocomposite using super critical nitrogen as a blowing agent: control of microstructure," *Advances in Polymer Technology*, vol. 37, no. 8, pp. 3017–3026, 2018.

[19] H. Tian, Y. Yao, S. Ma, J. Wu, and A. Xiang, "Enhanced thermal stability and flame resistance of polyurethane-imide foams by adding silicon carbide," *Advances in Polymer Technology*, vol. 37, no. 7, pp. 2470–2477, 2018.

[20] T. Liu, C. Lin, J. Liu et al., "Phase evolution, pore morphology and microstructure of glass ceramic foams derived from tailings wastes," *Ceramics International*, no. 12, pp. 14393–14400, 2018.

[21] S. Liu, Z. Li, Y. Li, and W. Cao, "Strength properties of Bayer red mud stabilized by lime-fly ash using orthogonal experiments," *Construction and Building Materials*, vol. 166, pp. 554–563, 2018.

[22] Z. Xi and A. Li, "Characteristics of thermoplastic powder in an aqueous foam carrier for inhibiting spontaneous coal combustion," *Process Safety and Environmental Protection*, vol. 104, pp. 268–276, 2016.

[23] A. Hajimohammadi, T. Ngo, and P. Mendis, "Enhancing the strength of pre-made foams for foam concrete applications," *Cement and Concrete Composites*, vol. 87, pp. 164–171, 2018.

[24] W. H. Chan, M. N. Mazlee, Z. A. Ahmad, M. A. M. Ishak, and J. B. Shamsul, "Effects of fly ash addition on physical properties of porous clay-fly ash composites via polymeric replica technique," *Journal of Material Cycles and Waste Management*, vol. 19, no. 2, pp. 794–803, 2016.

[25] A. Hajimohammadi, T. Ngo, and P. Mendis, "How does aluminium foaming agent impact the geopolymer formation mechanism?" *Cement and Concrete Composites*, vol. 80, pp. 277–286, 2017.

[26] M. Lassinantti Gualtieri, A. Cavallini, and M. Romagnoli, "Interactive powder mixture concept for the preparation of geopolymers with fine porosity," *Journal of the European Ceramic Society*, vol. 36, no. 10, pp. 2641–2646, 2016.

[27] W.-B. Liu and X. Zhang, "Study on volume stability of chemical foaming cement paste," *KSCE Journal of Civil Engineering*, vol. 21, no. 7, pp. 2790–2797, 2017.

[28] E. Papa, V. Medri, D. Kpogbemabou et al., "Porosity and insulating properties of silica-fume based foams," *Energy and Buildings*, vol. 131, pp. 223–232, 2016.

[29] L. C. Drake, "Pore-size distribution in porous materials," *Industrial & Engineering Chemistry Research*, vol. 16, no. 3, pp. 463–472, 2002.

[30] B. D. Zdravkov, J. J. Čermák, M. Šefara, and J. Janků, "Pore classification in the characterization of porous materials: a perspective," *Central European Journal of Chemistry*, vol. 5, no. 4, pp. 1158–1158, 2007.

[31] J. Kodikara, S. Barbour, and D. Fredlund, "Changes in clay structure and behaviour due to wetting and drying," 1999.

[32] K. K. Schiller, "Strength of porous materials," *Cement & Concrete Research*, vol. 1, no. 4, pp. 419–422, 1971.

[33] J. C. Taylor and C. E. Matulis, "Absorption contrast effects in the quantitative XRD analysis of powders by full multiphase profile refinement," *Journal of Applied Crystallography*, vol. 24, no. 1, pp. 14–17, 1991.

[34] M. Y. J. Liu, U. J. Alengaram, M. Santhanam, M. Z. Jumaat, and K. H. Mo, "Microstructural investigations of palm oil fuel ash and fly ash based binders in lightweight aggregate foamed geopolymer concrete," *Construction and Building Materials*, vol. 120, pp. 112–122, 2016.

[35] C. Tennakoon, A. Shayan, K. Sagoecrentsil, and J. G. Sanjayan, "Importance of reactive SiO_2, AlO_3 and Na_2O in geopolymer formation," *Austroads Bridge Conference*, 2014.